Energy Gap and Surface Structure of $YBa_2Cu_3O_{7-x}$ Probed by Scanning Tunneling Microscopy

H. L. Edwards, J. T. Markert, and A. L. de Lozanne
Department of Physics, University of Texas, Austin, Texas 78712-1081
(Received 29 July 1992)

We report the results of scanning tunneling microscopy (STM) and spectroscopy (STS) studies on high-quality single crystals of $YBa_2Cu_3O_{7-x}$ (YBCO) which were cleaved *in situ* at 20 K prior to measurement. STS reveals an energy gap with $2\Delta/kT_c = 6$–8 and conductance curves with small zero bias conductance. STM images show for the first time the complex atomic structure of the YBCO surface; atomic resolution disappears after heating to 70 K. Large features may be due to the electronic effects of oxygen disorder, and YBCO is shown to cleave between the BaO and CuO chain layers.

PACS numbers: 74.50.+r, 61.16.Di, 74.70.Vy

Tunneling has long been used to probe the basic properties of superconductors. Materials problems, however, have slowed the successful application of this technique to high-temperature superconductors (HTSC). In particular, scanning tunneling microscopy (STM) and scanning tunneling spectroscopy (STS) of $YBa_2Cu_3O_{7-x}$ (YBCO) have met with limited success due to the material's poor surface quality. For instance, it is well known that the YBCO surface degrades in air [1].

It has also been observed that the YBCO surface is unstable at 300 K in ultrahigh vacuum (UHV). Photoemission experiments by List *et al.* [2] on cold-cleaved $EuBa_2Cu_3O_{7-x}$ show a loss of intensity at the Fermi level when the sample is thermally cycled through 80 K; this is attributed to loss of chain oxygen at the cleaved surface, reducing it to insulating $EuBa_2Cu_3O_6$. A more recent study on YBCO [3] indicates that the crystals must be cleaved below 40 K to retain surface oxygen. Work which attempted to disclaim the view that the YBCO surface is unstable at 300 K, based on measurements of a Fermi edge at 300 K [4], did not address the question of whether the surface degrades on warming above 40 K.

There have been a number of STM and STS measurements on YBCO reported [5], but few have claimed vacuum tunneling [6] and none have achieved reproducible atomic resolution. We have obtained extensive atomic images of cold-cleaved (20 K) YBCO single crystals, and measured *I-V* curves which display a reproducible energy gap of $2\Delta/kT_c = 6$–8. This combination of atomic resolution and reproducible spectroscopy lends us confidence that, for the first time, the tunneling takes place through a well-characterized vacuum barrier.

Single crystals were grown by standard flux-based techniques in yttria-stabilized-zirconia crucibles. Millimeter-sized platelets were separated from the flux and annealed for six weeks in oxygen. SQUID magnetometer measurements in a field $H = 10$ Oe with H perpendicular to c indicate a 100% diamagnetic transition above 90 K, a 10%–90% transition width of 1 K about $T_c = 92$ K, and diamagnetic fraction $-4\pi\chi = 0.6$ and 1.0 for field-cooled and zero-field-cooled data, respectively. The crystals were glued between pieces of wire and cleaved *in situ* at 20 K.

STS yields current-voltage (*I-V*) curves, and was performed on several different samples, at many locations on each sample; one *I-V* curve is shown in the solid curve of Fig. 1. All samples were cleaved in our UHV, low-temperature STM [7] prior to measurement. Atomic-resolution STM was performed before and after some of the *I-V* curves were taken, and the junction resistance was above 1 GΩ for most curves. As seen in the inset of Fig. 1, the current $I(z)$ showed exponential behavior with distance z for the range of bias voltages and junction resistances used in taking the *I-V* curves. Note the roughly constant magnitude of the noise over the range, indicating that it is vibrational rather than electronic in origin. By measuring the logarithmic slope of $I(z) = I_0 \exp(-1.025\phi^{1/2} z)$, the barrier height ϕ was found to be about 1 eV for a freshly cleaved surface and 0.5 eV for a degraded surface.

As can be seen by the dotted curve of Fig. 1, the peaks in our differential conductance $[G(V) = dI/dV]$ curves are very broad. Because this broadening shifts peaks to higher energies, several techniques have been employed to measure the gap from these broadened conductance curves [5]. The simplest is to measure the distance between the conductance peaks, $2\Delta_{pp}$. The next simplest is to extrapolate the asymptotic conductance through the peak until it intersects the gap wall, the position of which

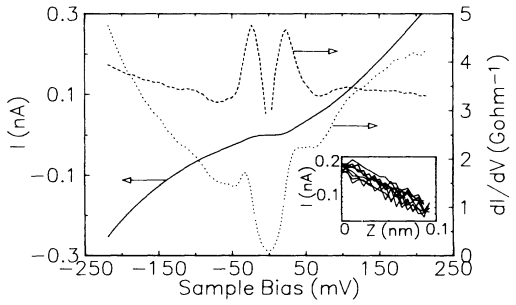

FIG. 1. The solid curve is the average of 128 *I-V* curves taken at the same location, at 20 K (4 mV, 9 pA offset subtracted). The dotted curve is the conductance dI/dV. The dashed curve is $R(V) = [(dI/dV)/(I/V)]^{1/2}$; the peak positions give 0.9Δ. Inset: The exponential dependence of the tunnel current (logarithmic scale) on height (linear scale) as the tip traversed the 0.1-nm path 8 times.

TABLE I. Energy gap values estimated by the various analysis techniques explained in the text. The critical temperature of the crystals is 92 K. Γ is only defined for the Dynes model.

	Δ (meV)	$2\Delta/kT_c$	No. curves used	Γ (meV)
Δ_{pp}	30 ± 8	6–10	37	...
Δ_{int}	20 ± 6	3–7	37	...
Δ_{Dynes}	21 ± 7	4–7	24	12 ± 4
Δ_R	28 ± 8	6–8	42	...

gives Δ_{int}. The final method is to fit the conductance curves to a Dynes depairing model [8], and extract both the energy gap Δ_{Dynes} and the broadening parameter Γ. Our gap estimates and parameter values obtained using these analyses are shown in Table I.

Unfortunately, none of these techniques is satisfactory for estimating the energy gap, as seen in the large spread of values in Table I. Δ_{pp} overestimates the energy gap by as much as 50% to 100% in highly broadened curves. Δ_{int} may be more accurate, but is difficult to measure when the conductance background is not constant. Δ_{Dynes} avoids overestimation, but offers no prescription for treating the nonconstant asymptotic conductance in the fit.

A technique which avoids all of these problems is to locate the peaks in the ratio of the differential conductance to the ordinary conductance [9], namely, $R=[(dI/dV)/(I/V)]^{1/2}$. R is plotted for I-V data as the dashed curve of Fig. 1. In calculating R, we subtracted the amplifier offset current and a small bias voltage sweep synchronization offset.

We take the square root in R since in the limit of no broadening, R equals the density of states $N(eV)$ for $|eV|>\Delta$. The advantage of using R to estimate the energy gap is pragmatic: The position of the peak in $R(V)$ is independent of the broadening. This is $(0.9\pm0.15)\Delta$, for $kT/\Delta=0.05$–0.15 and any amount of depairing broadening. Effects such as a nonconstant conductance background are factored out in $R(V)$. We call the gap estimated by this technique Δ_R, and its average value for our data is listed in Table I. We take the result of this analysis as our gap estimate, $2\Delta/kT_c=2\Delta_R/kT_c=6$–$8$.

In the dashed curve of Fig. 1, there are dips in R just outside the gap shoulders (at about 50–70 mV). These are calculational figments due to the nonconstant conductance background, and are not density-of-states features. A similar dip in $R(V)$ can be produced by numerically integrating the tunneling current equation with a tunneling matrix element proportional to V or V^2 to emulate the conductance background.

Our STS results share some of the anomalous features seen in other tunneling studies of HTSC [5,10]. Most $G(V)$ curves exhibit a linear conductance background ranging over more than 100 meV. Some curves exhibit nearly no zero-bias conductance $G(0)$, and the overall average is quite small: $G(0)/G(100\text{ meV})=(0.2\pm0.1)$.

Figure 2 shows an atomic image of a freshly cleaved sample. The features repeat in detail on subsequent images, and they do not vary in shape or orientation with scanning frequency. This and other images show a complex surface structure, with a simple feature: All of the atoms line up along parallel lines separated, within experimental error, by the a-direction lattice constant of 0.4 nm. Only the CuO chain layer displays such a preferred direction in the bulk, so we interpret these parallel lines as the CuO chains. This is, to the best of our knowledge, the first real-space observation of the CuO chains in YBCO. Figure 3 shows two images taken 100 nm apart,

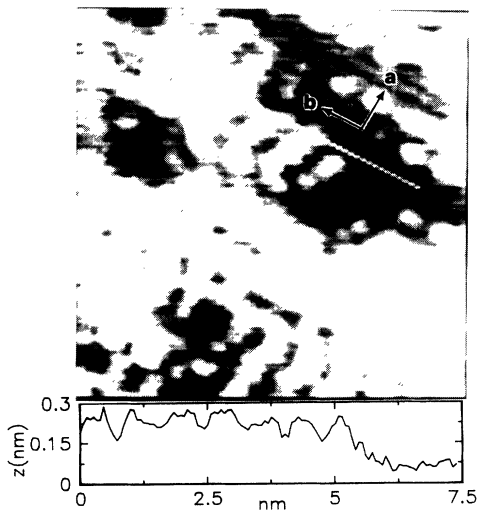

FIG. 2. An image of YBCO taken at 24 K, 7.5 nm on a side. Note that the atomic corrugations line up along rows in one direction (along line—corrugations shown in plot), but not the other direction. We take the rows parallel to the white line to be the CuO chains. Horizontal streaks are due to a vibrational noise. The image was taken at +200-mV sample bias and 50-pA average tunneling current.

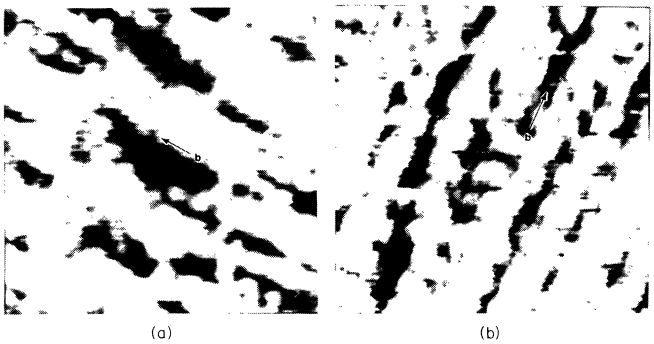

FIG. 3. (a) and (b) are taken near each other, but the CuO chains are perpendicular, indicating the existence of a twin boundary between these two images. These images are 7.5 nm on a side, and were taken at +1-V sample bias with an average tunneling current of 50 pA.

which are members of a set of 72 similar images taken along a 72-nm line. The chain orientation in Fig. 3(a) is shifted by 90° relative to that in Fig. 3(b), indicating that a twinning boundary exists between these two images.

Warming a freshly cleaved YBCO sample briefly (0.5 h) to 70 K was found to destroy the atomic resolution, particularly the chainlike features. Such measurements were done without crashing or macroscopically moving the tip, and such areas had been thoroughly mapped previously, with clear atomic resolution. Images before and after such a thermal cycle are shown in Fig. 4. In addition, ϕ decreased from 1 to 0.5 eV after the thermal cycle. This observation was repeated, and similar results obtained on a crystal cleaved at 70 K and cooled quickly to 20 K; this was done to check for sample contamination due to heater outgassing. Throughout this experiment, many as-prepared YBCO thin films and single crystals, uncleaved or cleaved at $T > 60$ K, have been studied, and atomic resolution was never obtained. Only the cold-cleaved single crystals have the pristine surface necessary for atomic-resolution STM, in agreement with the results of List *et al.* [2].

In the atomic images, steps of various heights were observed. Some steps were shorter than the YBCO unit cell c-direction height of 1.2 nm, indicating that cleaved YBCO shows several terminations. Figure 5 shows a 0.4-nm step in which the top layer has atomic resolution, but the bottom layer is featureless. This type of step seems to be very common for cleaved YBCO, and there were several highly stepped regions in one sample which displayed the following sequence: atomic resolution, tall step (0.8–1.0 nm) up; featureless layer, short step (0.3–0.5 nm) up; atomic resolution, tall step up, and so on.

In a simple model of HTSCs, the CuO chain layer donates holes to the CuO_2 planes [11]. The YBCO unit cell has two mirror symmetry planes perpendicular to the c axis: the CuO chain layer and the Y layer between the two CuO_2 planes. Thus, any particular cleavage plane in the unit cell has a symmetric equivalent plane which leaves a different surface exposed in cleave. If cleavage occurs, for instance, between BaO and CuO, then there will be regions of CuO chain-terminated surface, and regions in which the chains have been peeled away to reveal BaO covering the CuO_2 planes. Similarly, if the cleavage occurs between BaO and CuO_2, there will be regions of BaO-terminated surface and regions in which the BaO-CuO-BaO layer has been peeled away to reveal the top CuO_2 plane.

In the bulk, each CuO chain layer contributes half of its doping to the CuO_2 plane layer above it and half to the one below it, so we expect a surface terminating in a CuO chain layer (or CuO chain layer covered by BaO) to be overdoped, and a surface terminating in a CuO_2 plane layer (or CuO_2 plane layer covered by BaO) to be underdoped. The former regions should show up better than the underdoped regions on STM images, since they are more metallic. This is consistent with our observation of short steps up to clear images of chains, and tall steps up to featureless images. Since the steps up to the atomically resolved layers are short, and the atomic resolution has chainlike features, we conclude that the crystal structure naturally cleaves between the CuO chain layer and the BaO layer, exposing the chains and leaving short steps.

The STM results presented here shed light on other surface-sensitive studies. Liu *et al.* [12] and Fowler *et al.* [4] employed photoemission spectroscopy and x-ray photoelectron spectroscopy, respectively, to study cleaved single crystals of YBCO. They detected two Ba chemical states—a bulk one and a surface one—indicating a BaO-terminated structure. Tanaka *et al.* [13] used low-

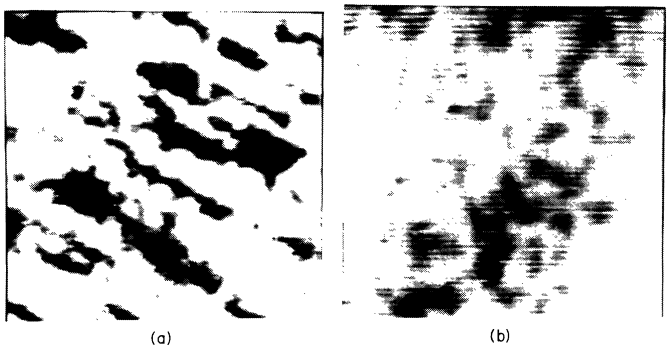

FIG. 4. Images taken at 24 K with the same tunneling parameters as in Fig. 3 (a) before and (b) after thermally cycling the sample to 70 K. Note the disappearance of atomic corrugations, particularly the CuO chains.

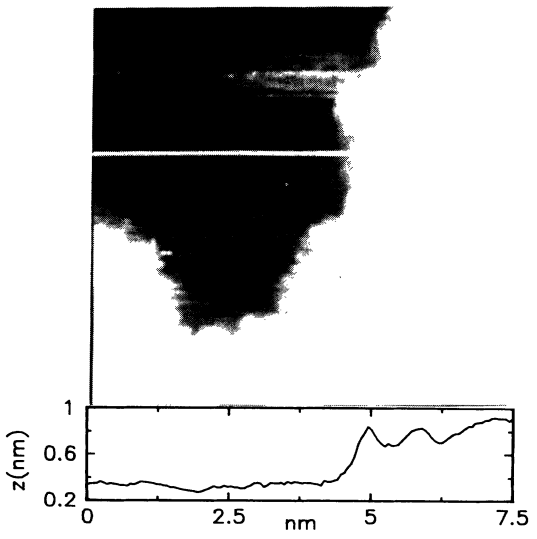

FIG. 5. Atomic image, 7.5 nm on a side, taken with +1-V sample bias and 50-pA tunneling current. Shown is a 0.4-nm step from a flat, featureless region up to a region which shows atomic corrugation similar to those in Figs. 2, 3, and 4(a). A cross section along the white line is plotted.

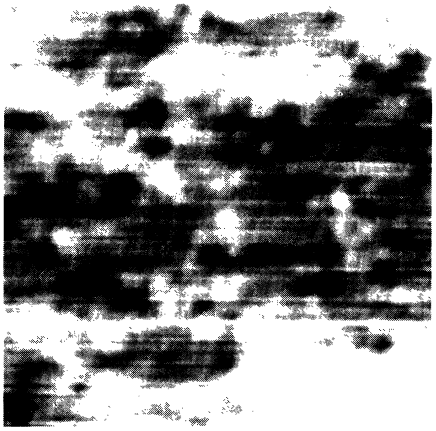

FIG. 6. An image, 15 nm on a side, taken at the large sample bias of +1 V, with 50-pA average current. Note the large, 1–2-nm swells and depressions; these bear no simple geometrical relation to the atomic structure measured at smaller bias values, and may be related to the electronic effects of oxygen disorder.

energy ion scattering spectroscopy to examine the scattering of ions from Ba atoms on the surface of YBCO, and found a "shadow" in the scattering which they attributed to a chain oxygen atom diagonally above each Ba at the surface. These two observations indicate the presence of both BaO-terminated and CuO chain-terminated areas on the YBCO surface. Our images show precisely this mixture of terminations.

Large scans at high sample bias show broad swells and depressions. These features, shown in Fig. 6, repeat in overlapping scans, and are independent of scanning frequency, so are real. They do not appear to bear a simple relation to observed atomic features, e.g., a depression does not correspond to a missing atomic layer.

CuO chain oxygen disorder alters the metallic properties of YBCO [11], and has been shown to set the critical temperature [14]. From formal valence counting, it can be seen that removing or adding an oxygen atom, or shifting its coordination about the chain copper atom, modifies the hole doping of the CuO_2 planes. A certain degree of frozen-in oxygen disorder could lead to spatial variations in the metallic properties of the CuO_2 planes. A variation of this sort may cause the large features seen in Fig. 6. This has also been observed in oxygen-deficient BiSrCaCuO [15].

In summary, we cleaved high-quality single crystals of YBCO to obtain clear atomic-resolution STM and sensible STS with $2\Delta/kT_c = 6$–8. YBCO cleaves between the BaO and CuO chain layers, as the chainlike features in the atomic images testify. The rich nature of the atomic topography reconciles a variety of features deduced from several surface-sensitive spectroscopies. We have directly confirmed the conclusion of List *et al.* [2] that the cleaved surface of YBCO is unstable except at very low temperatures by observing the disappearance of atomic corrugations on thermally cycling a freshly cleaved sample to 70 K. Finally, we observed large swells and depressions which may indicate electronic effects of oxygen disorder.

This work was supported by the Robert A. Welch Foundation under Grant No. F-1191 (J.T.M.), the National Science Foundation under Grants No. DMR-9158089 (J.T.M.) and No. DMR-8553305 (A.L.dL.), the Texas Advanced Technology Project (A.J.dL.), and the John A. Wheeler Fellowship (H.L.E.).

[1] R. P. Vasquez, M. C. Foote, B. D. Hunt, and L. Bajuk, J. Vac. Sci. Technol. A **9**, 570 (1991).
[2] R. S. List *et al.*, Phys. Rev. B **38**, 11966 (1988).
[3] J. C. Campuzano *et al.*, Phys. Rev. Lett. **64**, 2308 (1990).
[4] D. E. Fowler, C. R. Brundle, J. Lerczak, and F. Holtzberg, J. Electron. Spectrosc. Relat. Phenom. **52**, 323 (1990).
[5] T. Hasegawa, H. Ikuta, and K. Kitizawa, in Physical Properties of High Temperature Superconductors III, edited by D. M. Ginsburg (World Scientific, Singapore, to be published).
[6] S. L. Pryadkin and V. S. Tsoi, Pis'ma Zh. Eksp. Teor. Fiz. **49**, 268 (1989) [JETP Lett. **49**, 305 (1989)].
[7] S. Pan, Ph.D. thesis, University of Texas at Austin, 1991.
[8] R. C. Dynes, V. Narayanamurti, and J. P. Garno, Phys. Rev. Lett. **41**, 1509 (1978).
[9] J. A. Stroscio, R. M. Feenstra, and A. P. Fein, Phys. Rev. Lett. **57**, 2579 (1986).
[10] J. R. Kirtley, Int. J. Mod. Phys. B **4**, 201 (1990).
[11] J. K. Burdett, Physica (Amsterdam) **191C**, 282 (1992).
[12] R. Liu *et al.*, Phys. Rev. B **40**, 2650 (1989).
[13] S. Tanaka *et al.*, Appl. Phys. Lett. **59**, 3637 (1991).
[14] J. D. Jorgensen *et al.*, Physica (Amsterdam) **167C**, 571 (1990).
[15] Z. L. Wu, Y. L. Wang, Z. Zhang, and C. M. Lieber, Phys. Rev. B **43**, 8729 (1991).

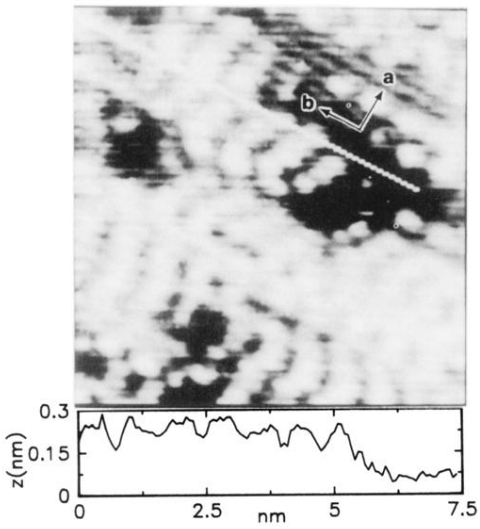

FIG. 2. An image of YBCO taken at 24 K, 7.5 nm on a side. Note that the atomic corrugations line up along rows in one direction (along line—corrugations shown in plot), but not the other direction. We take the rows parallel to the white line to be the CuO chains. Horizontal streaks are due to a vibrational noise. The image was taken at +200-mV sample bias and 50-pA average tunneling current.

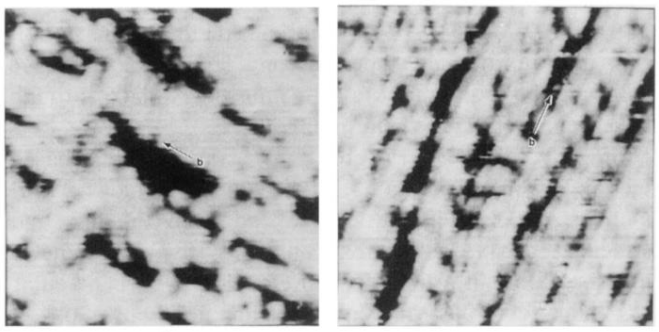

(a) (b)

FIG. 3. (a) and (b) are taken near each other, but the CuO chains are perpendicular, indicating the existence of a twin boundary between these two images. These images are 7.5 nm on a side, and were taken at +1-V sample bias with an average tunneling current of 50 pA.

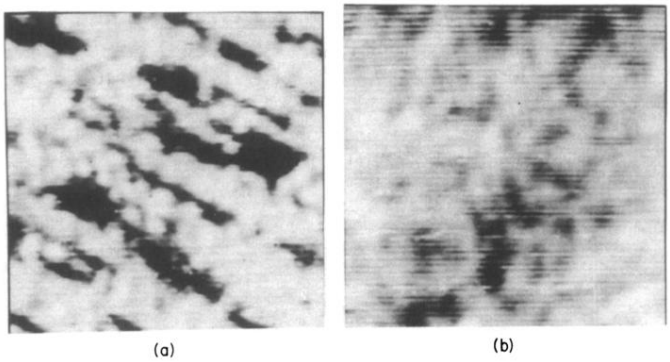

FIG. 4. Images taken at 24 K with the same tunneling parameters as in Fig. 3 (a) before and (b) after thermally cycling the sample to 70 K. Note the disappearance of atomic corrugations, particularly the CuO chains.

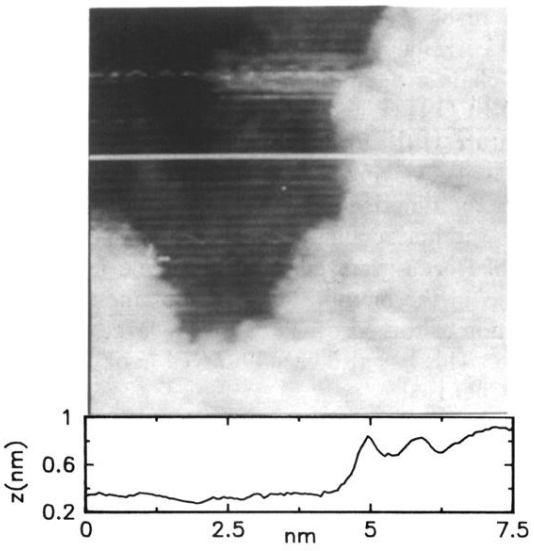

FIG. 5. Atomic image, 7.5 nm on a side, taken with +1-V sample bias and 50-pA tunneling current. Shown is a 0.4-nm step from a flat, featureless region up to a region which shows atomic corrugation similar to those in Figs. 2, 3, and 4(a). A cross section along the white line is plotted.

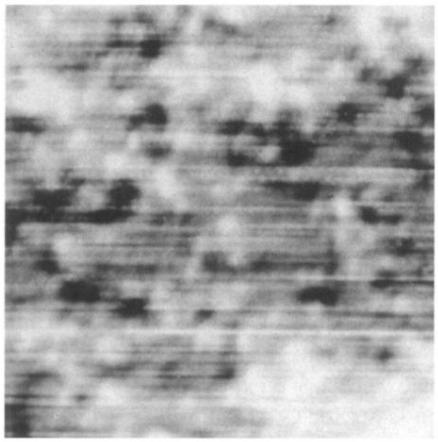

FIG. 6. An image, 15 nm on a side, taken at the large sample bias of +1 V, with 50-pA average current. Note the large, 1–2-nm swells and depressions; these bear no simple geometrical relation to the atomic structure measured at smaller bias values, and may be related to the electronic effects of oxygen disorder.